Nano Research

Open Access

Research Article

Garlic-derived nanoparticles inhibit tumor by activating tumor-infiltrating γδT cells

Jialu Xu[1,2,§], Jintao Huang[1,§], Yue Yu[2], Di Hu[1], Yue Zhang[2], Huaxing Dai[2], Li You[2], Fang Xu[2], Jian Shen[1] ✉, and Chao Wang[2] ✉

[1] *Department of Interventional Radiology, The First Affiliated Hospital of Soochow University, Suzhou 215006, China*
[2] *Institute of Functional Nano & Soft Materials (FUNSOM), Jiangsu Key Laboratory for Carbon-based Functional Materials and Devices, Soochow University, Suzhou 215123, China*
[§] *Jialu Xu and Jintao Huang contributed equally to this work.*

Cite this article: *Nano Research*, **2025**, *18*, 94907145. https://doi.org/10.26599/NR.2025.94907145

ABSTRACT: γδT cells have emerged as a promising target in tumor therapy, prompting the development of novel strategies to activate these cells directly within the tumor microenvironment. In this study, we engineered uniformly sized spherical garlic-derived nanoparticles (GNPs) to stimulate tumor-infiltrating γδT cells. Through intratumoral injection of GNPs, we demonstrated their ability to directly activate γδT cells, leading to potent antitumor effects. This approach resulted in significant inhibition of various subcutaneous tumors in mice. Additionally, under computed tomography (CT) guidance, intratumoral injection of GNPs effectively suppressed the growth of orthotopic liver cancer in New Zealand white rabbits. Mechanistic studies revealed that GNPs robustly activated γδT cells, promoting an inflammatory microenvironment within tumors. Our approach of using garlic-derived nanoparticles offers the advantages of simplicity in preparation and high yield, presenting a promising avenue for tumor therapy with potential for clinical translation.

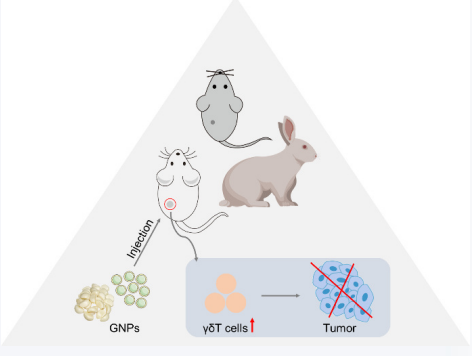

KEYWORDS: garlic-derived nanoparticles, γδT cells, tumor microenvironment, antitumor effects

1 Introduction

T cells are pivotal in the treatment of tumors. T cells can be categorized into two types based on their receptors: αβT cells and γδT cells [1]. αβT cells are the prevalent T cells that recognize and respond to tumor antigens, but the activation of αβT cells requires the help of antigen-presenting cells. Defects within DCs in the tumor microenvironment (TME) restrict the ability of $DC\text{-}CD8^+$ T cell cross-talk, leading to impaired $CD8^+$ T cells differentiation and function. In contrast, the activation of γδT cells does not require antigen-presenting cells and is not restricted by the major histocompatibility complex (MHC) [2–4]. Upon activation, γδT cells release a substantial amount of cytokines, increasing their cytotoxicity against tumor cells, and thereby facilitating tumor cell eradication [5–7]. At the same time, γδT cells are part of the innate immune system, possess antitumor activity, and are capable of directly recognizing and killing tumor cells. In recent years, γδT-based tumor treatment has become a prominent research focus [8–11]. Despite advancements leading to clinical use, numerous challenges persist in γδT cell-based tumor treatment, including the survival and persistence of γδT cells *in vivo* [12]. Activating tumor-infiltrating γδT cells directly is crucial for effective immunotherapy.

Plant-derived nanovesicles have emerged as a prominent research focus in the biological field due to their abundant sources and excellent biocompatibility [13–15]. The main components of plant-derived nanoparticles include lipids, proteins, DNA, and RNA [16]. Notably, nanoparticles have been successfully obtained from a variety of plants, including ginger, lemon, blueberry, and others [17–19]. They play a crucial role in the prevention and treatment of various diseases [20–22]. Currently, the approaches utilized to obtain plant-derived nanovesicles mainly include ultracentrifugation and density gradient centrifugation, and each extraction method has the limitations [23]. Therefore, new technologies need to be developed for the preparation, storage, and application of plant-derived nanoparticles.

Garlic has been widely utilized by humans as a seasoning since ancient times. Garlic contains a variety of active compounds,

Received: September 2, 2024; **Revised:** October 21, 2024
Accepted: November 19, 2024

✉Address correspondence to Jian Shen, shenj@suda.edu.cn; Chao Wang, cwang@suda.edu.cn

including allicin, polyphenols, and organic sulfides. These components confer various beneficial functions such as enhancing immunity, regulating immune cell activity, and exhibiting antioxidant and antitumor properties [24, 25]. In our previous study, we discovered that oral administration of garlic-derived nanoparticles (GNPs) effectively activated intestinal IFNγ-producing γδT cells [26]. GNPs stimulated endogenous γδT cells to inhibit tumor growth without no obvious toxicity, which could overcome the challenges faced in γδT cell-based tumor therapy. Here, we employed a simple method by crushing and high-pressure homogenization to obtain a large number of uniform nanovesicles from garlic, which were freeze-dried into powder and stored at room temperature with good stability. By intratumoral injection of GNPs, we revealed that GNPs can directly stimulate tumor-infiltrating γδT cells to elicit antitumor effects. A significant inhibitory effect on various subcutaneous tumors in mice was observed. At the same time, under the guidance of computed tomography (CT), intratumoral injection of GNPs also well suppressed the growth of orthotopic liver cancer in New Zealand white rabbits. The garlic-derived nanovesicles we prepared through a simple and easy-to-operate approach showed good antitumor effects, and have certain clinical translation potential.

2 Experimental

2.1 Materials

The antibodies and other materials utilized in this study were listed in Table S1 in the Electronic Supplementary Material (ESM).

2.2 Cell lines

DC2.4 (fh1026), RAW264.7 (TCM13), Jurkat (E6-1), B16-F10 (TCM36), CT26 (TCM37), and 4T1 (TCM32) cell lines were obtained from the Cell Bank at the Shanghai Institutes for Biological Sciences, Chinese Academy of Sciences. DC2.4, CT26, Jurkat, and 4T1 cells were cultured in RPMI 1640 medium supplemented with 10% fetal bovine serum (FBS), 100 U/mL penicillin, and 100 U/mL streptomycin. RAW264.7 and B16-F10 cells were cultured in Dulbecco's modified Eagle's medium (DMEM) supplemented with 10% FBS, 100 U/mL penicillin, and 100 U/mL streptomycin.

2.3 Mice

C57BL/6 and BALB/C female mice (6–8 weeks) were acquired from Changzhou Cavins Laboratory Animal Company. New Zealand white rabbits were procured from Zhen Hu Company. All animal experiments involving mice and New Zealand white rabbits were conducted in compliance with the approved protocols of our university laboratory animal center (Approval number: SUDA20210201A02; SUDA20230718A03) and adhered to the guidelines established by animal welfare regulatory authorities. The maximum allowable tumor burden for mice was set at 1500 mm^3, while for New Zealand white rabbits, it was 10,000 mm^3.

2.4 Preparation and characterization of garlic-derived nanoparticles

A certain amount of garlic purchased from the market was processed through a juicer at room temperature, followed by further crushing at 4 °C via a high-pressure homogenizer (1500 bar) to obtain GNPs. The prepared GNPs were freeze-dried into powders and stored at room temperature. The morphology of GNPs was studied using transmission electron microscopy (TEM), and the particle size distribution was characterized by a Zetasizer nano ZS particle size analyzer. The protein distribution of GNPs was analyzed by sodium dodecyl sulfate-polyacrylamide gel electrophoresis (SDS-PAGE). The allicin content of GNPs was measured via high-performance liquid chromatography (HPLC). To ensure the reproducibility of the preparation of GNPs, we monitored the particle size distribution, morphology, and allicin content of each prepared GNPs.

2.5 Cytotoxicity assay *in vitro*

The cytotoxicity of GNPs at different concentrations on dendritic cells (DC2.4), macrophages (RAW264.7), T cells (Jurkat), melanoma cells (B16-F10), colon cancer cells (CT26), and breast cancer cells (4T1) was evaluated by the standard MTT assay. Specifically, 10,000 cells were seeded into a 96-well plates. After 12 h, the supernatant was removed, and different concentrations of GNPs were added to the wells. The plate was then placed in an incubator for 24 h. Afterward, 20 μL of 5 mg/mL MTT solution was added to each well and incubated for 4 h. The medium containing the MTT solution was then removed, and 100 μL of dimethylsulfoxide (DMSO) solution was added to each well. The plate was placed on a shaker in the dark for 10 min. Finally, the absorbance at 570 nm was measured using a microplate reader. The concentrations of GNPs tested were 0, 25, 50, 75, 100, 125, 250, and 500 μg/mL.

2.6 T cell activation *in vitro*

Cy5.5-NHS and GNPs were incubated for 2 h at room temperature, and free Cy5.5-NHS was removed by ultracentrifugation. Cy5.5 and Cy5.5 labeled GNPs were incubated with αβT cells and γδT cells for 24 h, and then analyzed relative fluorescence intensity of Cy5.5 in αβT cells (PE-CD4, PE-CD8) and γδT cells (PE-TCR γ/δ) by flow cytometry. At the same time, the uptake of GNPs by αβT cells and γδT cells was observed through confocal microscopy. Briefly, Cy5.5 and Cy5.5 labeled GNPs were incubated with αβT cells and γδT cells for 24 h, followed by fixation with 4% paraformaldehyde for 15 min in phosphate buffer saline (PBS). After washing twice and finally staining with 4',6-diamidino-2-phenylindole (DAPI) for 15 min and washing three times with PBS, the uptake of GNPs by each cell was observed by a Zeiss confocal microscopy. After GNPs were incubated with intestinal-derived T cells for 24 h, T cells were collected by centrifugation at 1200 rpm for 3 min. Then αβT cells (FITC-CD3, APC-CD4, PE-CD8), and γδT cells (FITC-CD3, PE-TCR γ/δ) were analyzed by flow cytometry.

2.7 Therapeutic experiment of garlic-derived nanoparticles

On day 0, B16 melanoma tumor cells (10^6) were inoculated on one side of the back of C57BL/6 mice, while 4T1 breast tumor cells (2×10^6) were inoculated on one side of the back of BALB/c mice. When the tumor volume reached approximately 100 mm^3, intratumoral injection of GNPs was administered once every two days at a dosage of 25 mg/kg for a total of 5 times. Throughout the treatment course, tumor volume and body weight of the mice were monitored every two days until either the mice died or the tumor volume reached 1500 mm^3.

On the day following the final intratumoral injection, the mice were euthanized, and the tumors of mice in each group were

collected for immune evaluation and analysis. The specific procedure was as follows: The collected tumor tissues were prepared into single-cell suspensions, followed by flow cytometry antibody staining of corresponding immune cells, including γδT cells (APC-CD45, FITC-CD3, and PE-TCRγ/δ). After incubation at room temperature for 1 h, flow cytometry was applied to analyze immune cells in each group.

On day 0, VX2 tumors were inoculated into the livers of New Zealand white rabbits under CT guidance to establish an orthotopic liver cancer model. On the 10th day, CT was utilized to observe the growth of liver tumors. And at the same time, under the guidance of CT, GNPs were injected into the tumor at a dose of 25 mg/kg, once every two days for a total of 5 times. During the treatment, CT was used to observe and measure liver tumor volume to evaluate the efficacy of intratumoral injection of GNPs. At the same time, we also applied magnetic resonance imaging (MRI) to evaluate the efficacy of GNPs treatment.

2.8 Single-cell RNA sequencing of tumor

To analyze the changes of major cells in the tumor microenvironment, single-cell RNA-sequencing was performed from the tumor of UNTX and GNPs group. Single-cell suspensions were created by enzymatic digestion of the tumor tissues. Using the droplet segmentation feature of the Chromium Single Cell Controller (10× Genomics) system in the NCI-CCR single cell analysis tool, the oligo-dT-based complementary DNA database was barcoded. After removing dead cells and adjusting the cell concentration to the desired level, the machine detected about 10,000 cells. Sequencing was conducted using an Illumina NovaSeq system at the NCI-CCR sequencing facility. The OmicStudio tool, which can be found at https://www.omicstudio.cn/tool, was used to conduct bioinformatics analysis.

2.9 Biosafety of garlic-derived nanoparticles

To assess potential adverse effects of intratumoral injection of GNPs, we euthanized the treated mice and New Zealand white rabbits. We harvested major organs, including the heart, liver, spleen, lung, and kidney, and performed H&E staining. Additionally, blood samples were collected from New Zealand white rabbits on days 10, 17, and 24. After centrifugation to obtain serum, levels of alanine aminotransferase, aspartate aminotransferase, urea, and creatinine were analyzed to evaluate the function of liver and kidney in New Zealand white rabbits after intratumoral injection of GNPs.

2.10 Statistical analysis

All results were expressed as means ± SD. Unless otherwise stated, biological replicates were applied for all experiments. Two groups were compared using Student's *t*-test (two-tailed). All statistical analyses were performed using GraphPad Prism (8.0). In animal survival analyses, log-rank tests were used to determine statistical differences (**** $P < 0.0001$; *** $P < 0.001$; ** $P < 0.01$; * $P < 0.05$).

3 Results

3.1 Preparation and characterization of garlic-derived nanoparticles

To obtain GNPs, we first crushed the garlic with a juicer, and then utilized a low-temperature and high-pressure homogenizer to further extract the GNPs (Fig. 1(a)). We characterized the prepared GNPs by TEM and dynamic light scattering (DLS). The TEM image (Fig. 1(b)) revealed that the GNPs had a uniform distribution and a regular spherical appearance, with a particle size of approximately 120 nm. The DLS results (Fig. 1(c)) also showed the same phenomenon as the TEM image. After obtaining the GNPs, we freeze-dried them to produce powdered GNPs. We discovered that the yield of GNPs was roughly 10% (wt./wt.) (Fig. 1(d)). To explore the stability of the GNPs, we redissolved the GNPs powders in PBS and found that the GNPs powders had good solubility (Fig. 1(e)). The TEM image demonstrated that the redissolved GNPs maintained uniformly distributed spherical form (Fig. 1(f)). Additionally, DLS revealed that the size of the redissolved GNPs was also around 120 nm (Fig. 1(g)). The SDS-PAGE results showed that the protein content of the GNPs did not change significantly after freeze-drying (Fig. 1(h)). HPLC analysis determined the allicin

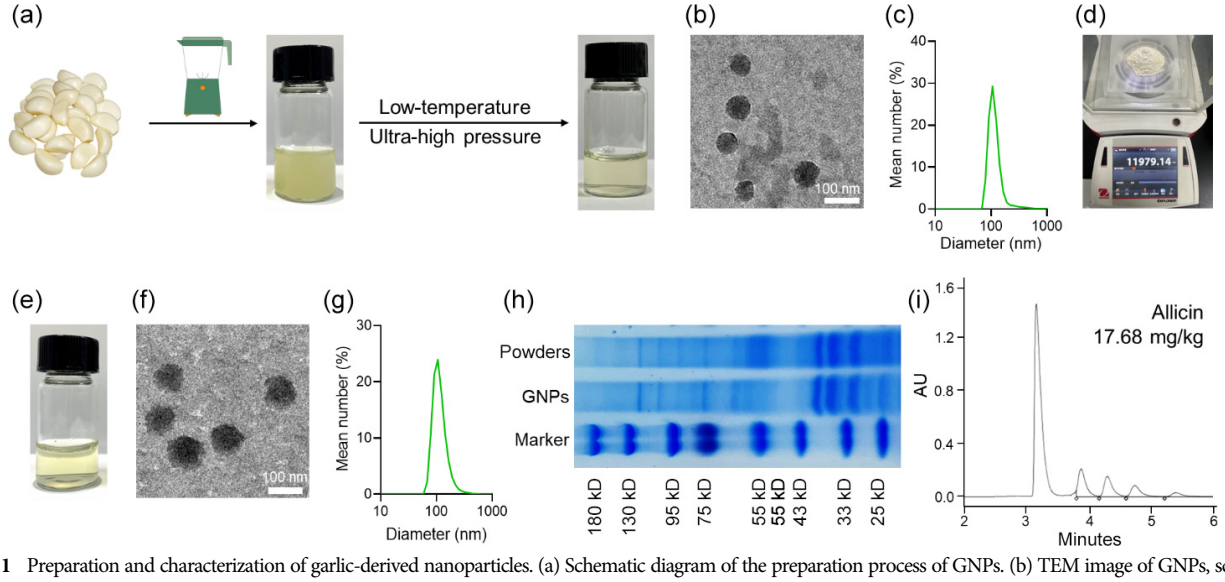

Figure 1 Preparation and characterization of garlic-derived nanoparticles. (a) Schematic diagram of the preparation process of GNPs. (b) TEM image of GNPs, scale bar = 100 nm. (c) DLS of GNPs. (d) Picture of powders of GNPs. (e) Picture of powders reconstituted in PBS. (f) TEM image of powders reconstituted in PBS, scale bar = 100 nm. (g) DLS of powders reconstituted in PBS. (h) Proteins of powders and GNPs. (i) Allicin content of GNPs. Data are means ± SD.

content of the GNPs was approximately 17.68 mg/kg (Fig. 1(i)). The above results indicated that the physical and chemical properties of the GNPs remained largely unchanged when they were stored in powder form.

Next, we verified the safety of GNPs in a variety of cells through an MTT assay. The results demonstrated that GNPs at different concentrations had no obvious cytotoxicity to immune cells and tumor cells, including dendritic cells, macrophages, T cells, B16 cells, CT26 cells, and 4T1 cells. It was evident that the GNPs we extracted were safe for a range of cells (Fig. S1 in the ESM).

We then investigated the impact of GNPs on T cells *in vitro*. Initially, we evaluated the uptake of GNPs by T cells by flow cytometry and confocal microscopy. According to the results of flow cytometry and confocal imaging, GNPs could be successfully taken up by γδT cells (Figs. 2(g) and 2(h)), but not by αβT cells (including CD4 T cells or CD8 T cells) (Figs. 2(a), 2(b), 2(d), and 2(e)). Moreover, following co-incubation with GNPs, there was a considerable increase in the proportion of γδT cells (Fig. 2(i)), while there was no significant change in the proportion of αβT cells (Figs. 2(c) and 2(f)). These results were in line with those of our previous study, indicating that GNPs can directly and effectively activate γδT cells.

3.2 Regulation of the tumor microenvironment by intratumoral injection of GNPs

The results of *in vitro* experiments indicated that γδT cells were directly activated by GNPs. Subsequently, we performed single-cell sequencing analysis of tumors after intratumoral injection of GNPs (25 mg/kg). The percentage of CD45 cells in the tumor dramatically increased following intratumoral injection, increasing to almost 1.8 times that of the untreated group (Figs. S2(a)–S2(c) in the ESM). After performing a thorough examination of the immune cells within the tumor, we conducted a detailed analysis of T cells in tumors, including CD4 T cells, CD8 T cells, NKT cells, and γδT cells (Figs. 3(a) and 3(b)). Based on the results of the tumor single cell sequencing, after intratumoral injection of GNPs, the number of γδT cells increased to a certain extent (Fig. 3(c)). Flow cytometry of tumors also showed the same results (Fig. 3(d) and Fig. S4 in the ESM). Meanwhile, activation markers of γδT cells were also upregulated, including *Cd69*, *Klrk1*, *Il2ra*, *Mapk1*, *Gzmb*, *Gzma*, *Prf1*, and *Mki67* (Fig. 3(e)). According to the cytokines secreted, γδT cells can be divided into two categories: IFN-γ-γδT cells and IL-17A-γδT cells. IFN-γ-γδT cells possess antitumor properties, while IL-17A-γδT cells promote tumor growth [2, 5, 7, 8]. By classifying γδT cells in tumors, we found that after intratumoral injection of GNPs, the proportion of IFN-γ-γδT cells increased significantly, while the proportion of IL-17A-γδT cells decreased (Figs. 3(f) and 3(g)). This demonstrated that GNPs contributed to the production of IFN-γ-γδT cells in tumors. Kyoto Encyclopedia of Genes and Genomes (KEGG) pathway analysis also demonstrated that after intratumoral injection of GNPs, γδT cells in tumors displayed antitumor activity, and genes related to these pathways were also upregulated (Figs. 3(h) and 3(i)). Moreover, we discovered that intratumoral injection of GNPs leads to the activation of other immune cells such as αβT cells (Fig. S5 in the ESM).

3.3 Therapeutic efficacy of intratumoral injection of GNPs

To evaluate the effect of intratumoral injection of GNPs on tumors, we conducted studies on mice melanoma model. When the tumor size reached approximately 100 mm^3, the GNPs were injected intratumorally, and the therapeutic efficacy was evaluated by measuring the tumor size (Fig. 4(a)). According to the tumor growth curve, intratumoral injection of GNPs had a superior inhibitory effect on melanoma in mice compared with the control mice (Figs. 4(b) and 4(c)), and extended their survival (Fig. 4(d)). Throughout the treatment, the body weight of the mice and H&E staining of major organs did not change significantly, suggesting

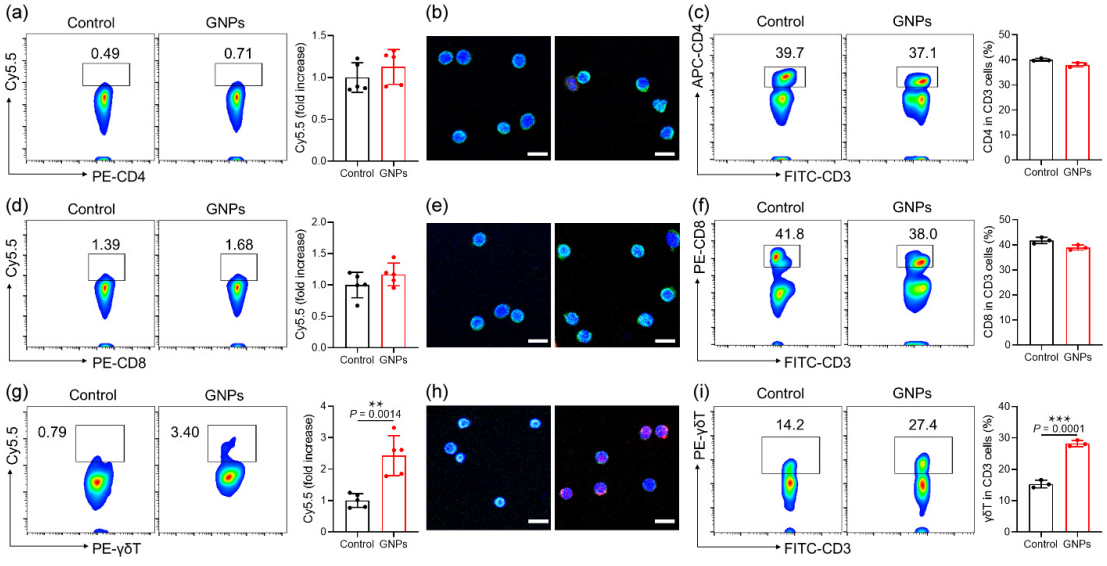

Figure 2 T cell activation *in vitro*. (a) Flow cytometry plots and fold increase of Cy5.5 signal in CD4 T cells in control and GNPs groups. (b) Confocal imaging of Cy5.5 signal on CD4 T cells after incubation Cy5.5-labelled GNPs (blue: DAPI; green: CD4 T cells; red: GNPs, scale bar = 20 μm). (c) Flow cytometry plots and quantitative analysis of CD4 T cells in CD3 cells in control and GNPs groups. (d) Flow cytometry plots and fold increase of Cy5.5 signal in CD8 T cells in control and GNPs groups. (e) Confocal imaging of Cy5.5 signal on CD8 T cells after incubation Cy5.5-labelled GNPs (blue: DAPI; green: CD8 T cells; red: GNPs, scale bar = 20 μm). (f) Flow cytometry plots and quantitative analysis of CD8 T cells in CD3 cells in control and GNPs groups. (g) Flow cytometry plots and fold increase of Cy5.5 signal in γδT cells in control and GNPs groups. (h) Confocal imaging of Cy5.5 signal on γδT cells after incubation Cy5.5-labelled GNPs (blue: DAPI; green: γδT cells; red: GNPs, scale bar = 20 μm). (i) Flow cytometry plots and quantitative analysis of γδT cells in CD3 cells in control and GNPs groups. *** $P < 0.001$; ** $P < 0.01$. Data are means ± SD.

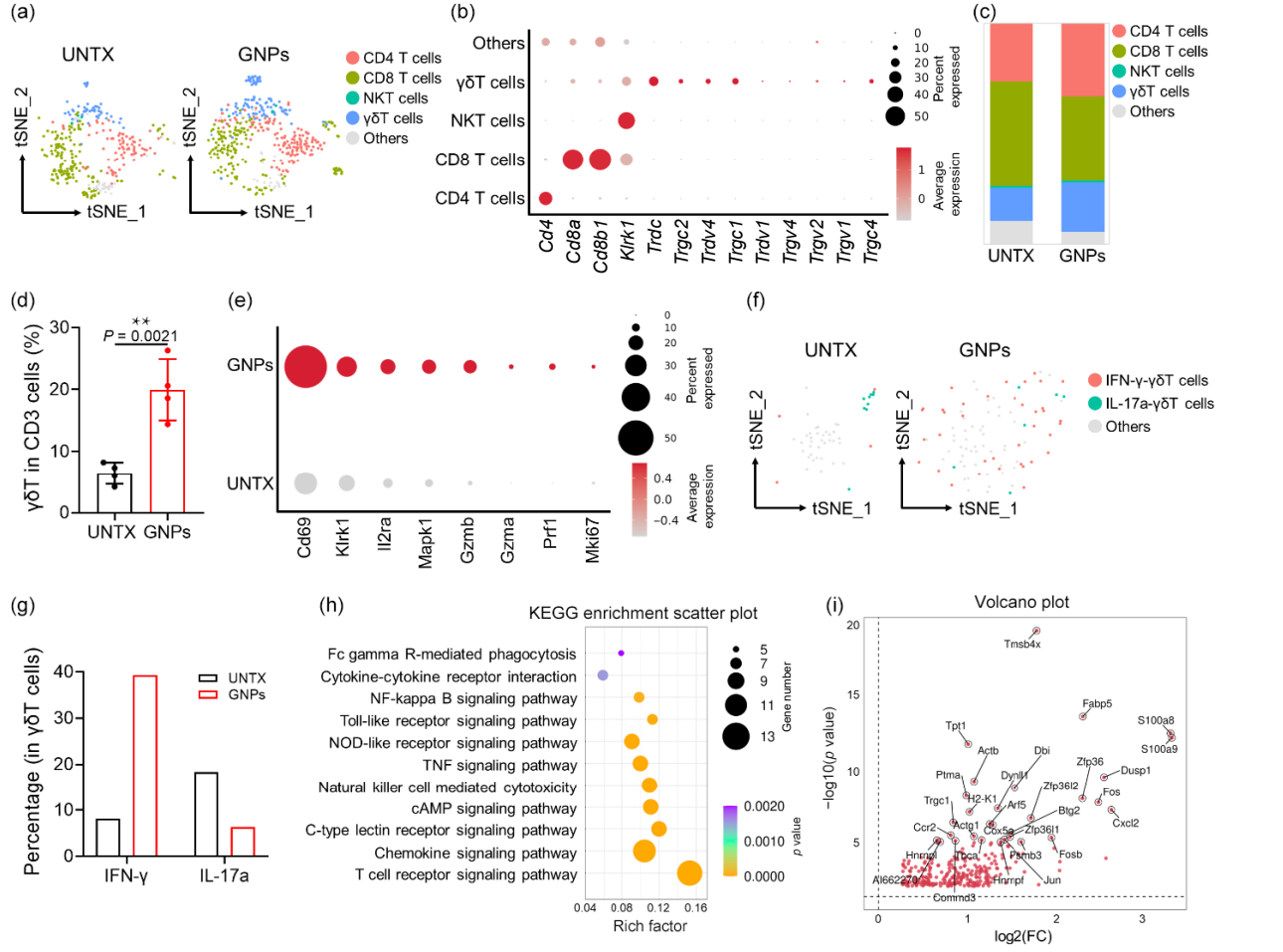

Figure 3 Single-cell sequencing analysis of T cells in tumor after GNPs intratumoral injection. (a) tSNE plot of different T cells in the UNTX group and GNPs group. (b) The main specific markers of different T cells, including CD4 T cells, CD8 T cells, NKT cells, and γδT cells. (c) Relative proportions of different T cells in the UNTX and GNPs groups. (d) Quantitative analysis of γδT cells in CD3 cells in UNTX and GNPs groups. (e) Relative expression of γδT cells activation markers in the UNTX and GNPs groups. (f) tSNE plot of γδT cells in the UNTX group and GNPs group. (g) Relative proportions of γδT cells in the UNTX and GNPs groups, including IFN-γ-γδT cells and IL-17a-γδT cells. (h) KEGG enrichment scatter plot of γδT cells in tumors. (i) Volcano plot of corresponding gene expression on γδT cells in tumors. ** $P < 0.01$. Data are means ± SD.

that GNPs therapy did not induce noticeable adverse effects (Fig. 4(e) and Fig. S6 in the ESM). Next, we implanted 4T1 breast tumor cells into BALB/c mice and treated them in accordance with the protocol established (Fig. 4(a)). Intratumoral injection of GNPs also effectively inhibited the growth of breast cancer (Figs. 4(f) and 4(g)) and substantially prolonged the survival of mice (Fig. 4(h)). Meanwhile, the body weight of BALB/c mice did not decrease during treatment (Fig. 4(i)). The above results of various tumor models indicated that intratumoral injection of GNPs was widely applicable for the treatment of tumors.

Considering the favorable therapeutic outcomes observed with intratumoral injection of GNPs in subcutaneous tumors in mice, we next inoculated VX2 tumors into the livers of New Zealand white rabbits to establish an orthotopic liver cancer model. Under the guidance of computed tomography (CT), we commenced intratumoral injection of GNPs into liver tumors every two days beginning on the 10th day post-implantation (Fig. 5(a)). To visually monitor the development of *in situ* liver cancer in New Zealand white rabbits, we performed CT imaging of liver tumors on days 10, 17, and 24. As shown in the CT images, the growth of orthotopic liver cancer was delayed after intratumoral injection of GNPs (Fig. 5(b)). The tumor growth curves also reflected tumor suppression after treatment (Figs. 5(c) and 5(d)). To better discern the alterations in liver tumors of New Zealand white rabbits after GNPs treatment, we employed diffusion-weighted imaging (DWI) and apparent diffusion coefficient (ADC) images of MRI to monitor hepatic conditions on day 24 (Fig. 5(e)). MRI demonstrated a notable increase in the ADC signal after GNPs treatment, indicating heightened tumor tissue liquefaction and necrosis (Fig. 5(f)). These findings revealed that liver tumors were effectively inhibited after intratumoral GNPs injection.

After intratumoral injection of GNPs, we euthanized New Zealand white rabbits and harvested major organs including the heart, liver, spleen, lung, and kidney for H&E staining. As depicted in the images, intratumoral GNPs injection exhibited no detrimental effects on major organs (Fig. 5(g)). Meanwhile, we collected the blood of New Zealand white rabbits from the UNTX and GNPs groups during the treatment. After serum was collected via centrifugation on various days (10, 17, and 24 days), the levels of alanine aminotransferase (ALT), aspartate aminotransferase (AST), urea (UREA), and creatinine (CREA) were monitored. The results showed that the indicators related to liver and kidney function did not change obviously during the treatment, suggesting the preservation of liver and kidney functions in New Zealand white

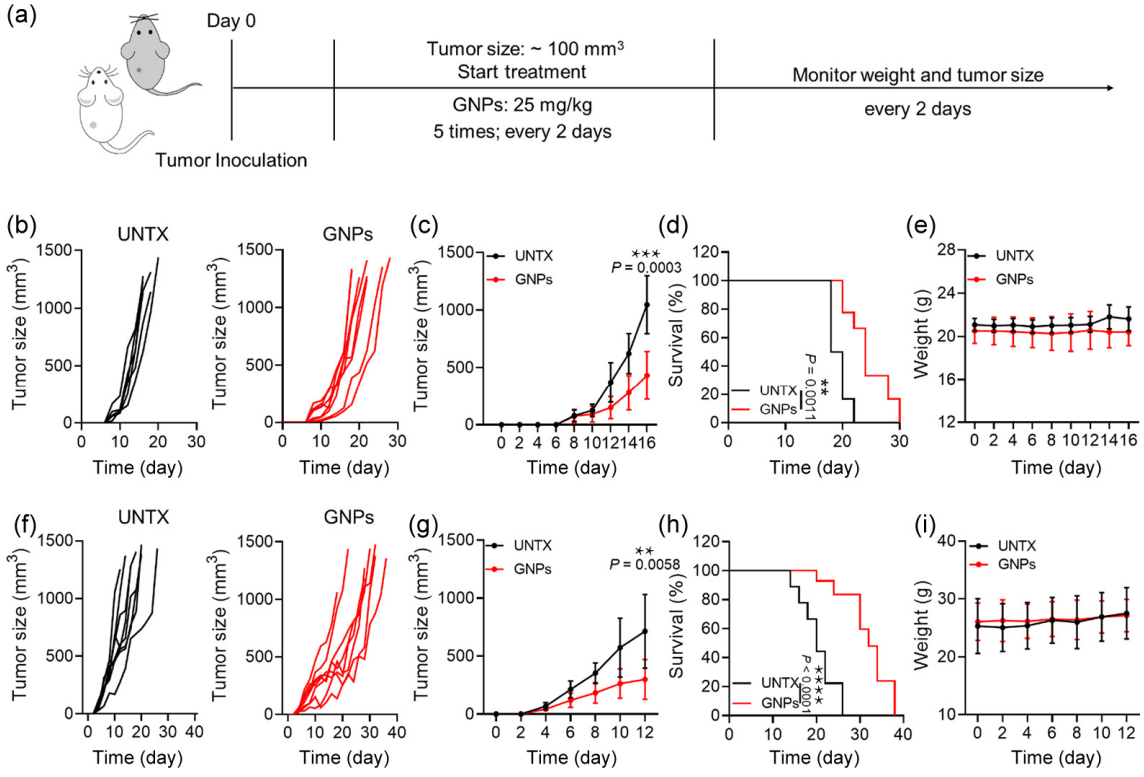

Figure 4 Intratumoral injection of GNPs for the treatment of mice. (a) Schematic diagram of the treatment process. (b) Tumor growth curve of each C57BL/6 mouse in the UNTX and GNPs group. (c) Average tumor growth curves of C57BL/6 mice in the UNTX and GNPs group. (d) Survival curves of C57BL/6 mice in the UNTX and GNPs group. (e) Weight growth curves of C57BL/6 mice in the UNTX and GNPs group. (f) Tumor growth curve of each BALB/C mouse in the UNTX and GNPs group. (g) Average tumor growth curves of BALB/C mice in the UNTX and GNPs group. (h) Survival curves of BALB/C mice in the UNTX and GNPs group. (i) Weight growth curves of BALB/C mice in the UNTX and GNPs group. **** $P < 0.0001$; *** $P < 0.001$; ** $P < 0.01$. Data are means ± SD.

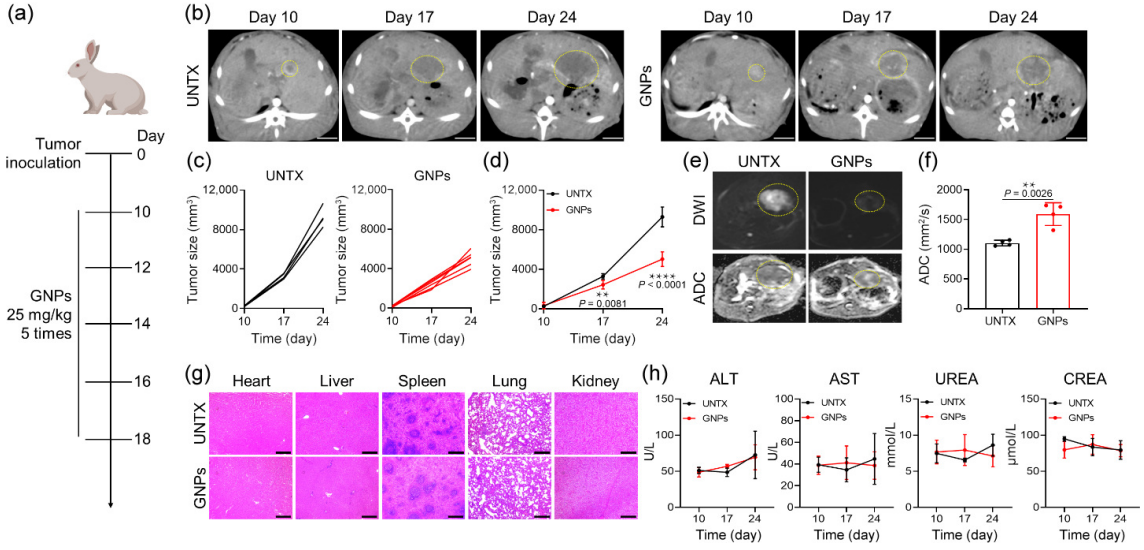

Figure 5 Intratumoral injection of GNPs for the treatment of orthotopic liver tumor in New Zealand white rabbits. (a) Schematic diagram of the treatment process. (b) CT images of the liver tumor in the UNTX and GNPs group on days 10, 17, and 24. Scale bar = 10 mm. (c) Tumor growth curve of each rabbit in the UNTX and GNPs group. (d) Average tumor growth curves of rabbits in the UNTX and GNPs group. (e) MRI of the liver in the UNTX and GNPs group on day 24. (f) Quantitative analysis of ADC values from MRI. (g) H&E staining of major organs in the UNTX and GNPs group, including heart, liver, spleen, lung, and kidney. Scale bar = 100 μm. (h) Time-varying curve of alanine aminotransferase, aspartate aminotransferase, urea, and creatinine in serum. **** $P < 0.0001$; ** $P < 0.01$. Data are means ± SD.

rabbits (Fig. 5(h)). These findings confirmed the relative safety of intratumoral GNPs injection under the guidance of CT.

4 Conclusions

In this study, we applied a simple and easy-to-operate method to extract nanoparticles from garlic for directly activating tumor-infiltrating γδT cells. We utilized a low-temperature and high-pressure homogenizer preparation technology to large-scale prepare the GNPs. Through intratumoral injection of GNPs, superior antitumor efficacy has been demonstrated in various subcutaneous tumor models in mice and orthotopic liver cancer models in New

Zealand white rabbits. The GNPs we prepared can directly activate endogenous γδT cells, which to a certain extent overcomes the challenges of γδT cell-based tumor therapy and has certain clinical translation capabilities. Future clinical applications of GNPs can involve combining them with existing tumor treatment strategies, such as immune checkpoint inhibitors, chemotherapy or radiotherapy. Such combination therapies may enhance overall treatment efficacy by leveraging the ability of GNPs to boost γδT cell activity while minimizing adverse effects. Moreover, the broader implications for immunotherapy are significant, as GNPs provide a novel approach to enhancing endogenous immune responses, potentially improving outcomes in patients who are unresponsive to current therapies.

Electronic Supplementary Material: Supplementary material (the antibodies and other materials utilized in this study and supplementary figures in this text) is available in the online version of this article at https://doi.org/10.26599/NR.2025.94907145.

Data availability

All data needed to support the conclusions in the paper are presented in the manuscript and the Electronic Supplementary Material. Additional data related to this paper may be requested from the corresponding author upon request.

Acknowledgments

This work was supported by the National Key R&D Program of China (No. 2022YFB3808100) and the National Natural Science Foundation of China (No. 32371476). This work was partly supported by the Collaborative Innovation Center of Suzhou Nano Science & Technology, the Priority Academic Program Development of Jiangsu Higher Education Institutions (PAPD), and the 111 Project.

Declaration of Competing Interest

The authors declare no competing interests.

Author contribution statement

C. W., J. S., and J. L. X. designed the project. J. L. X. and J. T. H. performed the experiments and collected the data. J. L. X. and J. T. H. analyzed and interpreted the data. All authors contributed to the writing of the manuscript, discussed the results and implications, and edited the manuscript at all stages.

Informed consent

Not applicable.

Ethics statement

All animal experiments involving mice and New Zealand white rabbits were conducted in compliance with the approved protocols of Soochow University laboratory animal center (Approval number: SUDA20210201A02; SUDA20230718A03) and adhered to the guidelines established by animal welfare regulatory authorities.

Use of AI statement

None.

References

[1] Meng, F. Q.; Lin, Z. D.; Ma, Y. M.; Che, R. B.; Zhang, C.; Wei, Y. T.; Song, X.; Liang, X.; Zhang, X. D. Engineered algae microrobots as photosynthetic living materials promote T cells' anti-tumor immunity. *Cell Rep. Phys. Sci.* **2024**, *5*, 102023.

[2] Foord, E.; Arruda, L. C. M.; Gaballa, A.; Klynning, C.; Uhlin, M. Characterization of ascites- and tumor-infiltrating γδ T cells reveals distinct repertoires and a beneficial role in ovarian cancer. *Sci. Transl. Med.* **2021**, *13*, eabb0192.

[3] Chien, Y. H.; Konigshofer, Y. Antigen recognition by γδ T cells. *Immunol. Rev.* **2007**, *215*, 46–58.

[4] Wiesheu, R.; Coffelt, S. B. From backstage to the spotlight: γδT cells in cancer. *Cancer Cell* **2024**, *42*, 1637–1642.

[5] Mensurado, S.; Silva-Santos, B. J. T. Battle of the γδ T cell subsets in the gut. *Trends Cancer* **2022**, *8*, 881–883.

[6] Reis, B. S.; Darcy, P. W.; Khan, I. Z.; Moon, C. S.; Kornberg, A. E.; Schneider, V. S.; Alvarez, Y.; Eleso, O.; Zhu, C. X.; Schernthanner, M. J. S. et al. TCR-Vγδ usage distinguishes protumor from antitumor intestinal γδ T cell subsets. *Science* **2022**, *377*, 276–284.

[7] Widlund, H. R.; Lynch, L. γδ T cells as unconventional targets of checkpoint blockade. *Nat. Cancer* **2024**, *5*, 373–374.

[8] Yan, J. Antitumor γδ T cells need oxygen to function. *Nat. Immunol.* **2021**, *22*, 268–269.

[9] Hayday, A.; Tigelaar, R. Immunoregulation in the tissues by γδ T cells. *Nat. Rev. Immunol.* **2003**, *3*, 233–242.

[10] Carding, S. R.; Egan, P. J. γδ T cells: Functional plasticity and heterogeneity. *Nat. Rev. Immunol.* **2002**, *2*, 336–345.

[11] Arias-Badia, M.; Chang, R.; Fong, L. γδ T cells as critical anti-tumor immune effectors. *Nat. Cancer* **2024**, *5*, 1145–1157.

[12] Lin, T. D.; Rubinstein, N. D.; Fong, N. L.; Smith, M.; Craft, W.; Martin-McNulty, B.; Perry, R.; Delaney, M. A.; Roy, M. A.; Buffenstein, R. Evolution of T cells in the cancer-resistant naked mole-rat. *Nat. Commun.* **2024**, *15*, 3145.

[13] Lian, M. Q.; Chng, W. H.; Liang, J.; Yeo, H. Q.; Lee, C. K.; Belaid, M.; Tollemeto, M.; Wacker, M. G.; Czarny, B.; Pastorin, G. Plant-derived extracellular vesicles: Recent advancements and current challenges on their use for biomedical applications. *J. Extracell. Vesicles* **2022**, *11*, 12283.

[14] Liu, H.; Geng, Z.; Su, J. C. Engineered mammalian and bacterial extracellular vesicles as promising nanocarriers for targeted therapy. *Extracell. Vesicles Circ. Nucleic Acids.* **2022**, *3*, 63–86.

[15] Wu, B. D.; Pan, W. L.; Luo, S. H.; Luo, X. R.; Zhao, Y. T.; Xiu, Q.; Zhong, M. Z.; Wang, Z. X.; Liao, T.; Li, N. C. et al. Turmeric-derived nanoparticles functionalized aerogel regulates multicellular networks to promote diabetic wound healing. *Adv. Sci.* **2024**, *11*, 2307630.

[16] Rome, S. Biological properties of plant-derived extracellular vesicles. *Food Funct.* **2019**, *10*, 529–538.

[17] Nguyen, T. N. G.; Pham, C. V.; Chowdhury, R.; Patel, S.; Jaysawal, S. K.; Hou, Y. C.; Xu, H.; Jia, L.; Duan, A.; Tran, P. H. L. et al. Development of blueberry-derived extracellular nanovesicles for immunomodulatory therapy. *Pharmaceutics* **2023**, *15*, 2115.

[18] Qiao, Z. Z.; Zhang, K.; Liu, J.; Cheng, D. J.; Yu, B. R.; Zhao, N. N.; Xu, F. J. Biomimetic electrodynamic nanoparticles comprising ginger-derived extracellular vesicles for synergistic anti-infective therapy. *Nat. Commun.* **2022**, *13*, 7164.

[19] Yang, M.; Liu, X. Y.; Luo, Q. Q.; Xu, L. L.; Chen, F. X. An efficient method to isolate lemon derived extracellular vesicles for gastric cancer therapy. *J. Nanobiotechnol.* **2020**, *18*, 100.

[20] Kameli, N.; Dragojlovic-Kerkache, A.; Savelkoul, P.; Stassen, F. R. Plant-derived extracellular vesicles: Current findings, challenges, and future applications. *Membranes* **2021**, *11*, 411.

[21] Karamanidou, T.; Tsouknidas, A. Plant-derived extracellular vesicles as therapeutic nanocarriers. *Int. J. Mol. Sci.* **2022**, *23*, 191.

[22] Fang, W. L.; Jing, Z. Y.; Li, Y.; Zhang, Z. R.; Lin, Z. D.; Yang, Z. X.; Tian, Y. S.; Zhang, C.; Ma, Y. M.; Hou, L. L. et al. Harnessing enucleated cancer cells as Trojan horse cell vaccines. *Cell Rep. Phys. Sci.* **2024**, *5*, 101752.

[23] Nemati, M.; Singh, B.; Mir, R. A.; Nemati, M.; Babaei, A.; Ahmadi, M.; Rasmi, Y.; Golezani, A. G.; Rezaie, J. Plant-derived extracellular vesicles: a novel nanomedicine approach with advantages and challenges. *Cell Commun. Signal.* **2022**, *20*, 69.

[24] Khanum, F.; Anilakumar, K. R.; Viswanathan, K. R. Anticarcinogenic properties of garlic: A review. *Crit. Rev. Food Sci. Nutr.* **2004**, *44*, 479–488.

[25] Londhe, V. P.; Gavasane, A. T.; Nipate, S. S.; Bandawane, D. D.; Chaudhari, P. D. A. Role of garlic (*Allium sativum*) in various diseases: An overview. *J. Pharm. Res. Opin.* **2011**, *1*, 129–134.

[26] Xu, J. L.; Yu, Y.; Zhang, Y.; Dai, H. X.; Yang, Q. Y.; Wang, B. L.; Ma, Q. L.; Chen, Y. T.; Xu, F.; Shi, X. L. et al. Oral administration of garlic-derived nanoparticles improves cancer immunotherapy by inducing intestinal IFNγ-producing γδ T cells. *Nat. Nanotechnol.* **2024**, *19*, 1569–1578.